PID controller design for a novel multi-input multi-output boost converter hub

M Alzgool and H Nouri

Power Systems, Electronics and Control Research Laboratory, UWE Bristol, UK

Mais2.alzgool@live.uwe.ac.uk

ABSTRACT

This paper reports on the design, control, and modeling of a novel multi-input multi-output boost converter topology. The converter hub can integrate renewable energy sources such as wind turbines, photovoltaic arrays, and fuel cells for the provision of different output voltage levels. The advantage of energy sources integration is that the required output voltage levels could be made up from a range of sources. The designed converter has the advantages of a simple configuration, fewer components, high conversion ratio, and high efficiency. The regulated output voltage levels are achieved through classical PID controllers which utilize the concept of closed-loop voltage-mode control. Design of the converter control system requires comprehensive knowledge of the converter structure, its operation principle and the small-signal model for continuous-conduction operation mode. The validity of the converter's control performance is demonstrated through software simulation.

KEY WORDS**:** DC-DC Converter, Multi-Input Multi-Output (MIMO), Renewable energy, small signal modelling, state space averaging, Insulated Gate Bipolar Transistor (IGBT)

1. INTRODUCTION

Recently, the number of applications which require more than one power source or more than one kind of energy source is increasing. Generating multi-input converters, having the capability of diversifying different energy sources, will provide improved reliability and the system flexibility.

Many control methods are used for controlling DC-DC converters where the simple and low-cost controller structure is always in demand for most industrial and high-performance applications [1]. Most used technique to control switching power supplies is pulse width modulation [2].

When boost converter is employed in open loop mode, it exhibits poor voltage regulation and unsatisfactory dynamic response, and hence, this converter is provided with closed-loop control for output voltage regulation. Hence, various closed-loop techniques had been proposed such as PID controller, Fuzzy logic, and other techniques, as well as many other researchers came up with new designs to be controlled with appropriate control technique such as using soft switching technique [3,4] presented high-frequency power switches design and robust controller.

In controlling the DC-DC converters, a voltage mode control or current mode control could be applied simply by closing a feedback loop between the required output voltages and switching device's duty ratio signal [2]. Due to nonlinearity of current mode control dynamics, the difficulties of obtaining the small-signal model is achieved; furthermore, in current mode control, an additional inner feedback loop is needed to control the inductor current, and then the output voltage is regulated indirectly [5], thus the current mode control is more complex to implement than voltage mode control.

Within closed-loop system, PID control is considered as a traditional linear control method commonly used in many applications [6]. The PID controller is a popular control feedback used in industrial area due to its flexibility and easy implementation in real applications; furthermore, if the system is complex, the PID can be designed to track an error and assume the system as a black box. A PID controller calculates an error value as the difference between the measured value and the desired reference value [7], and by adjusting three parameters k_p, k_i, and k_d of the system which would affect the transient response, rise time, settling time and steady-state error, overshoot, and stability. Thus, it may not necessary for the system to utilize the three actions P, I, and D; it may use one or two actions to improve the system dynamic response.

In this paper, closed-loop voltage-mode control using a PID controller is employed to control the multi-input multi-output (MIMO) DC-DC boost converter topology structure as shown in Figure 1, where different input sources connected in such a way to integrate the available input sources to provide a high conversion ratio [8].

The paper organized as follows: Section 2 presents the proposed MIMO DC-DC boost converter topology with the mathematical representation for ideal and non-ideal converter. Furthermore, the operation principle of the proposed converter is presented in section 2. The dynamic modeling of the DC-DC boost converter for three-input source double output is presented in section 3 including the MATLAB simulation results. Finally, the conclusion of this study is summarized in section 4.

2. CONVERTER STRUCTURE AND OPERATION PRINCIPLES

A new design and efficient MIMO DC-DC boost converter is proposed with the specifications of high conversion ratio and lower number of components in comparison to the available MIMO boost converter topologies.

In this design, the stepping up voltage occurs in two stages, where the output voltage of the first stage (V_o) acts like the DC input voltage to the next stage, so that to provide a higher conversion ratio, which is important in high DC voltage applications.

The mathematical equations of the proposed MIMO boost converter have been derived assuming that the system is lossless (ideal components):

$$V_{o1} = \left[\frac{V_{i1}}{1-D_{i1}} + \frac{V_{i2}}{1-D_{i2}} + \frac{V_{i3}}{1-D_{i3}} + \ldots + \frac{V_{im}}{1-D_{im}}\right]\left[\frac{1}{1-D_{o1}}\right] \tag{1}$$

$$V_{on} = \left[\sum_{k=1}^{k=m} V_{ik}\frac{1}{1-D_{ik}}\right]\left[\frac{1}{1-D_{on}}\right] \tag{2}$$

Where,
V_{on} is the output DC voltage.
V_{ik} is the DC input voltage.

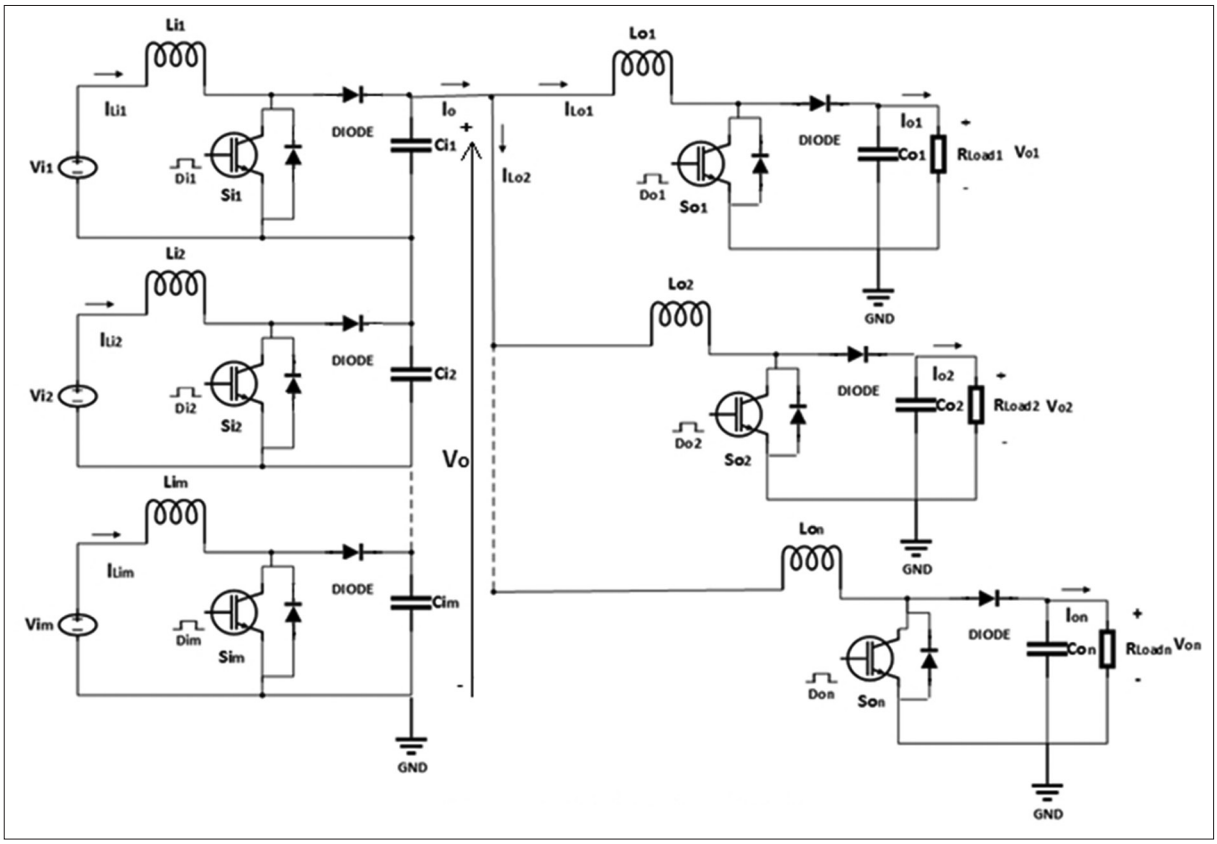

Figure 1. *Proposed multi-input multi-output DC-DC boost converter topology*

D_{ik} is the duty cycle of the input IGBT switches.
D_{on} is the duty cycle of the output IGBT switches.

From Equation (2), the conversion ratio of the proposed converter is expressed as:

$$\frac{V_{on}}{V_{im}} = \frac{m}{(1-Di)(1-Don)}; \text{ if } (D_{i1} = D_{i2} = D_{im} = D_i) \tag{3}$$

Where, m is the number of inputs of the proposed converter and n is the number of outputs.

If the conversion ratio of the proposed converter in Equation (3) is compared to the conversion ratio of the classical boost converter shown below in Equation (4).

$$\frac{V_o}{V_i} = \frac{1}{1-D} \tag{4}$$

It is noticeable that the conversion ratio of the proposed converter is much higher than the classical boost as shown in Figure 2. For example, the classical boost conversion ratio for 80% duty cycle will be 5 while, for the same condition, the conversion ratio of the proposed single-input single-output (SISO) boost converter will be 25, which means 5 times more than the classical boost conversion ratio. In the same figure, you can see how the conversion ratio increases as the number of inputs increase.

Where $(D_{i1} = D_{i2} = D_{im} = D_{on})$

Moreover, for non-ideal components, the mathematical equations of the proposed MIMO converter by the inductor volt-second balance approach have been derived. Thus, the general equation of the non-ideal (including losses) MIMO boost converter output voltage will be:

$$V_{on(non-ideal)} = \left[\frac{1}{1-D_{on}}\right]\left[\sum_{k=1}^{k=m} V_{ik}\frac{1}{1-D_{ik}}\right] - \left[\sum_{k=1}^{k=m} V_{S_{ik-ON}}\frac{1}{(1-D_{ik})(1-D_{on})} - \frac{1}{(1-D_{ik})(1-D_{on})}\right] - I_{L_k}\left(R_{S_{ik}} - R_{L_{ik}}\right) - V_{DIODE_{ik-ON}} \tag{5}$$

$$\left[\sum_{j=1}^{j=n} V_{S_{oj-ON}}\left(\frac{D_{oj}}{1-D_{oj}}\right) - I_{L_{oj}}R_{L_{oj}}\left(\frac{D_{oj}}{1-D_{oj}}\right) - V_{DIODE_{oj-ON}}\right]$$

Where,
$V_{S_{ik-ON}}$ is the input IGBT-ON state voltage drop which is between two to three volts.

$V_{S_{oj-ON}}$ is the output IGBT-ON state voltage drop which is between two to three volts.

$V_{DIODE_{k,oj-ON}}$ is the diode forward voltage.

$R_{S_{ik}}$ and R_{L_k} are the DC resistance of the voltage source and the inductor, respectively.
$I_{L_{ik,oj}}$ is the input and output inductor current.

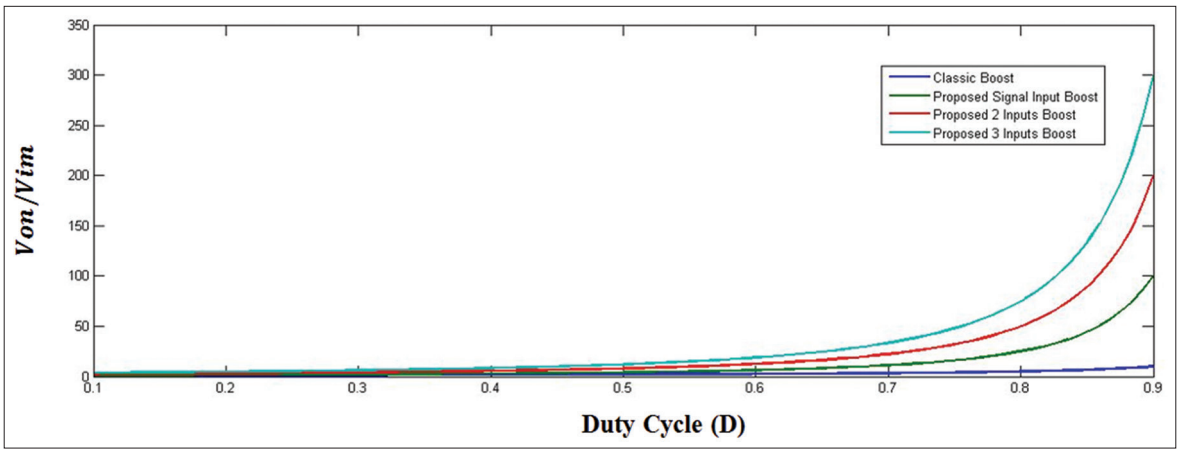

Figure 2. *Comparison between the conversion ratio of the proposed converter and the classical boost converter*

It is clear that the output voltage drops when the losses included, thus the converter's efficiency decreases [8], for example, if the efficiency of the proposed double inputs single output ideal converter 100%, then the efficiency of the non-ideal converter drops to reach 95.8% which is <4.2% of the ideal converter's efficiency due to losses. Figure 3 depicts the efficiency of the ideal and non-ideal converter with different number of outputs.

As the number of output increases the converter's efficiency decreases (for ideal and non-ideal converter) as more power switches conducted, and the output current will be reduced as the number of output increases to feed the whole loads. In spite of the losses of the proposed non-ideal converter, a high efficiency is acquired.

In this paper, three-input sources V_{i1}, V_{i2}, and V_{i3} are responsible for supplying the loads. The converter is designed to operate in continuous-conduction mode as the inductor current never reaches zero. In this mode, the five switches are active, and for each switch, a specific duty ratio is considered. Here, S_{i1} is active to regulate the first input source V_{i1} current to desired value. At the same time, S_{i2} and S_{i3} are active to regulate V_{i2}, V_{i3}, respectively, by controlling the input inductor currents IL_{i2} and IL_{i3}. By regulating the duty ratios of the input switches the DC bus voltage V_0 whrer ($V_0 = V_{c1} + V_{c2} + V_{c3}$). Furthermore, the output voltage V_{o1} is controlled by the output power switch S_{o1}; similarly, S_{o2} regulates the second output voltage V_{o2}. According to the switches' states, there are four different switching states in one switching period as shown in Figure 4. For each state, the inductor and capacitor equations have been investigated as follows:

a. Switching state 1: In this state, the switches on the input side S_{i1}, S_{i2}, and S_{i3} are turned ON, while the output switches S_{o1} and S_{o2} are turned OFF. When the input switches are ON, the input stage diodes are reversed biased, so S_{o1} and S_{o2} are OFF. Assuming that the output capacitors are fully charged, thus the power will deliver to the load R_{L1} and R_{L2}. The equivalent circuit of the proposed converter in this state is shown in Figure 4a. In this state, V_{i1}, V_{i2}, and V_{i3} charge the inductors L_{i1}, L_{i2}, and L_{i3}, respectively, so the inductors' current increases and the output capacitors are discharged.

   The equations for the inductors and capacitors in this mode are as follows:

$$\left.\begin{aligned}
L_{i1}\frac{di}{dt} &= v_{i1}\\
L_{i2}\frac{di}{dt} &= v_{i2}\\
L_{i3}\frac{di}{dt} &= v_{i3}\\
C_{i1}\frac{dv_{ci1}}{dt} &= -i_o\\
C_{i2}\frac{dv_{ci2}}{dt} &= -i_o\\
C_{i3}\frac{dv_{ci3}}{dt} &= -i_o\\
L_{o1}\frac{di}{dt} &= v_o - v_{co1}\\
L_{o2}\frac{di}{dt} &= v_o - v_{co2}\\
C_{o1}\frac{dv_{co1}}{dt} &= i_{Lo1} - \frac{v_{o1}}{R_{L1}}\\
C_{o2}\frac{dv_{co2}}{dt} &= i_{Lo2} - \frac{v_{o2}}{R_{L2}}
\end{aligned}\right\} \quad (6)$$

b. Switching state 2: In this state, the switches on the input side S_{i1}, S_{i2}, and S_{i3} are still ON, and the output switches S_{o1} and S_{o2} are turned ON. When the input switches are ON, the input stage diodes are reversed biased. Assuming that the output capacitors are fully charged, thus the power will deliver to the load R_{L1} and R_{L2}. The equivalent circuit of the proposed converter in this state is shown in Figure 4b. In this state, V_{i1}, V_{i2}, and V_{i3} charge the inductors L_{i1}, L_{i2}, and L_{i3}, respectively, also the output inductors L_{o1} and L_{o2} are charged from the capacitors C_{i1}, C_{i2}, and C_{i3}. Consequently, the inductors' current IL_{o1} and IL_{o2} increases. In addition, capacitors C_{o1} and C_{o2} are discharged. The equations for the inductors and capacitors in this mode are as follows:

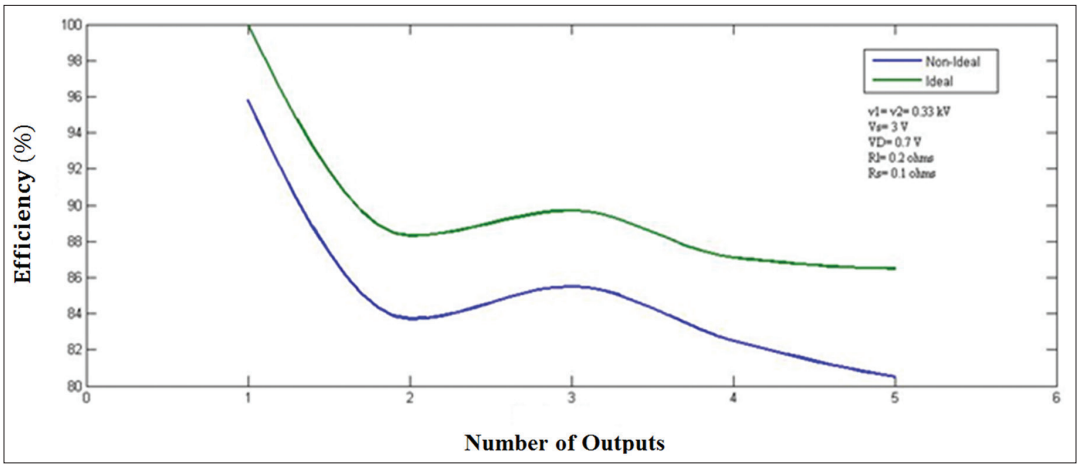

Figure 3. *The converter's efficiency of the ideal and non-ideal converter with different number of outputs*

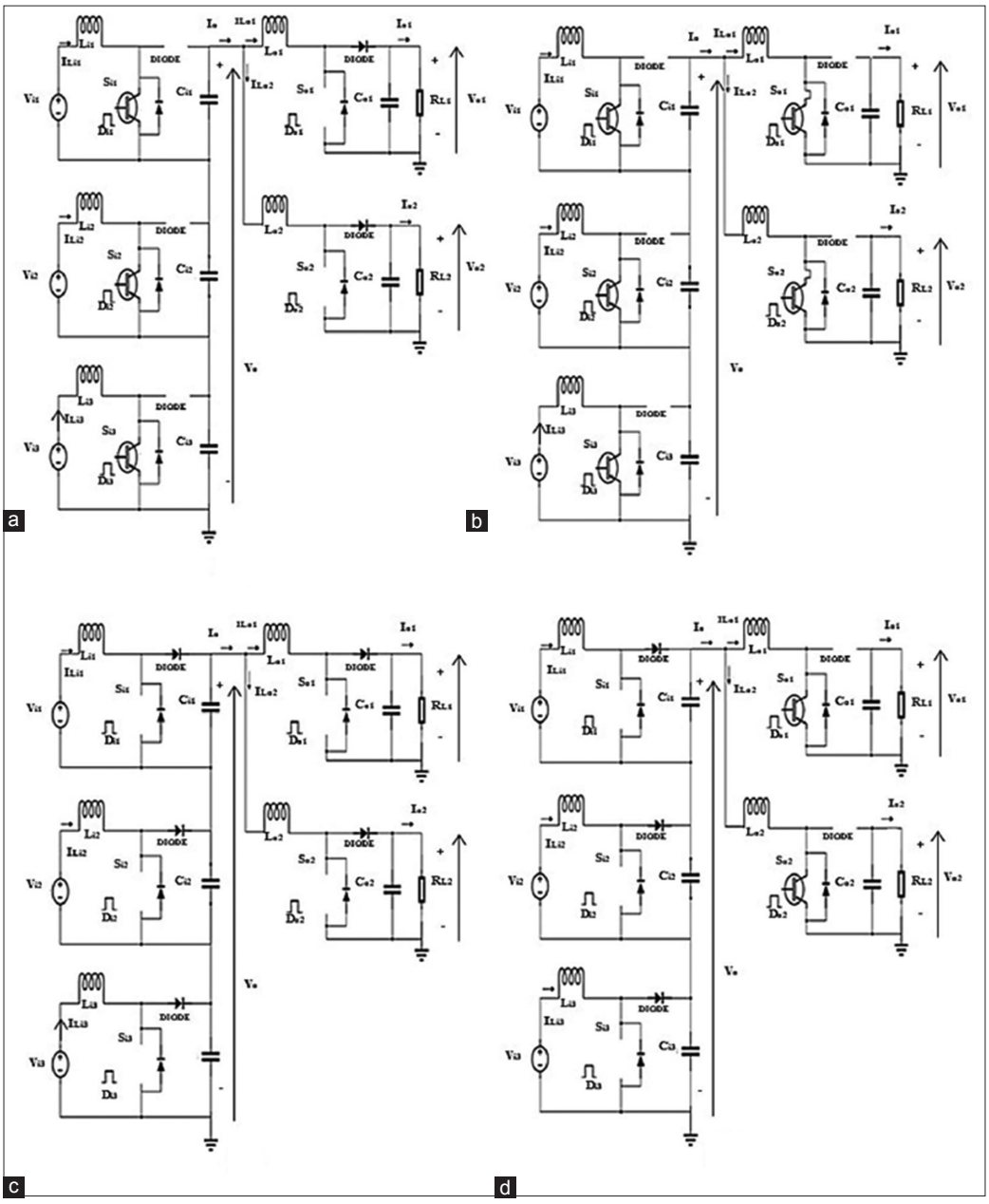

Figure 4. *Equivalent circuit of boost converter switching mode, (a) switching state 1, (b) switching state 2, (c) switching state 3, (d) switching state 4*

$$\left.\begin{aligned}
L_{i1}\frac{di}{dt} &= v_{i1}\\
L_{i2}\frac{di}{dt} &= v_{i2}\\
L_{i3}\frac{di}{dt} &= v_{i3}\\
L_{o1}\frac{di}{dt} &= v_{o}\\
L_{o2}\frac{di}{dt} &= v_{o}\\
C_{i1}\frac{dv_{ci1}}{dt} &= -\left(i_{Lo1}+i_{Lo2}\right)\\
C_{i2}\frac{dv_{ci2}}{dt} &= -\left(i_{Lo1}+i_{Lo2}\right)\\
C_{i3}\frac{dv_{ci3}}{dt} &= -\left(i_{Lo1}+i_{Lo2}\right)\\
C_{o1}\frac{dv_{co1}}{dt} &= \frac{-v_{o1}}{R_{L1}}\\
C_{o2}\frac{dv_{co2}}{dt} &= \frac{-v_{o2}}{R_{L2}}
\end{aligned}\right\} \quad (7)$$

c. Switching state 3: In this state, the switches on the input side S_{i1}, S_{i2}, and S_{i3} are turned OFF, and the output switches S_{o1} and S_{o2} are turned OFF. When the input switches are OFF, the input stage diodes are forward biased. In this state, the stored energy in the input inductors will deliver to charge the capacitors C_{i1}, C_{i2}, and C_{i3}. In addition, the stored energy in the output inductors will deliver to charge the output capacitors C_{o1} and C_{o2}, as well as to deliver the stored energy to the loads R_{L1} and R_{L2}. The equivalent circuit of the proposed converter in this state is shown in Figure 4c. In this state, the inductors' current IL_{i1}, IL_{i2}, and IL_{i3} decreases and the capacitors C_{i1}, C_{i2}, and C_{i3} charged. The equations for the inductors and capacitors in this mode are as follows:

$$\left.\begin{aligned}
L_{i1}\frac{di}{dt} &= v_{i1} - v_{ci1}\\
L_{i2}\frac{di}{dt} &= v_{i2} - v_{ci2}\\
L_{i3}\frac{di}{dt} &= v_{i3} - v_{ci3}\\
L_{o1}\frac{di}{dt} &= v_{o} - v_{co1}\\
L_{o2}\frac{di}{dt} &= v_{o} - v_{co2}\\
C_{i1}\frac{dv_{ci1}}{dt} &= i_{Li1} - i_{o}\\
C_{i2}\frac{dv_{ci2}}{dt} &= i_{Li2} - i_{o}\\
C_{i3}\frac{dv_{ci3}}{dt} &= i_{Li3} - i_{o}\\
C_{o1}\frac{dv_{co1}}{dt} &= i_{Lo1} - \frac{v_{o1}}{R_{L1}}\\
C_{o2}\frac{dv_{co2}}{dt} &= i_{Lo2} - \frac{v_{o2}}{R_{L2}}
\end{aligned}\right\} \quad (8)$$

d. Switching state 4: In this state, the switches on the input side S_{i1}, S_{i2}, and S_{i3} are still OFF, and the output switches S_{o1} and S_{o2} are turned ON. When the input switches are OFF, the input stage diodes are forward biased. In this state, the stored energy in the input inductors keeps charging the capacitors C_{i1}, C_{i2}, and C_{i3}. In addition, the stored energy in the input inductors will deliver to L_{o1} and L_{o2} through the switches S_{o1} and S_{o2}, respectively. Hence, the

inductors' current IL_{i1}, IL_{i2}, and IL_{i3} keep decreasing, while IL_{o1} and IL_{o2} increases. In addition, the capacitors C_{o1} and C_{o2} will discharge through the loads R_{L1} and R_{L2}. The equivalent circuit of the proposed converter in this state is shown in Figure 4d. The equations for the inductors and capacitors in this mode are as follows:

$$\left.\begin{aligned}
L_{i1}\frac{di}{dt} &= v_{i1} - v_{ci1}\\
L_{i2}\frac{di}{dt} &= v_{i2} - v_{ci2}\\
L_{i3}\frac{di}{dt} &= v_{i3} - v_{ic3}\\
L_{o1}\frac{di}{dt} &= v_o\\
L_{o2}\frac{di}{dt} &= v_o\\
C_{i1}\frac{dv_o}{dt} &= i_{Li1} - i_o\\
C_{i2}\frac{dv_o}{dt} &= i_{Li2} - i_o\\
C_{i3}\frac{dv_o}{dt} &= i_{Li3} - i_o\\
C_{o1}\frac{dv_{co1}}{dt} &= \frac{-v_{o1}}{R_{L1}}\\
C_{o2}\frac{dv_{co2}}{dt} &= \frac{-v_{o2}}{R_{L2}}
\end{aligned}\right\} \quad (9)$$

3. DYNAMIC MODEL OF THE DC-DC BOOST CONVERTER

The MIMO converter is controlled by switches S_{i1}, S_{i2}, S_{i3} and S_{o1}, S_{o2}. Each switch has its own specific duty cycle. By proper regulation of switches' duty cycles, the outputs voltage, namely, V_{o1} and V_{o2} can be adjusted. To design the closed-loop controller for the converter, it is necessary to obtain the dynamic model. As stated before in section 2, to control the output voltages, regulating the bus DC voltage V_o is also needed. In addition, as each input has its own power switch and different parameters values, thus different controllers need to be designed. Figure 5 depicts the control block diagram of the proposed converter with three inputs and two outputs.

Small-signal model is the basis for optimized controller design. Especially, for MIMO converters, an effective model will aid to realize closed-loop control and to optimize the converter dynamics [1]. Unlike the conventional SISO converters, the MIMO converter is a high order system, and the derivation of the plant transfer function is extensive; therefore, it is difficult to obtain values of poles and zeros for analysis.

The dynamics of the plant can be described in a matrix form. Based on small-signal modeling method [2], the state variables (x) and duty ratios (d), input voltages (v) contain two components, dc values (X, D, V) and disturbance values $(\hat{x},\hat{d},\hat{v})$. It is assumed that the perturbations are small and do not vary significantly during one switching period. Hence, the proposed converter equations are as follows:

$$\left.\begin{aligned}
i_{Li}(t) &= I_{Li} + \hat{i}_{Li}(t)\\
i_{Lo}(t) &= I_{Lo} + \hat{i}_{Lo}(t)\\
v_{o1}(t) &= V_{o1} + \hat{v}_{o1}(t)\\
v_{o2}(t) &= V_{o2} + \hat{v}_{o2}(t)\\
d_{i1}(t) &= D_{i1} + \hat{d}_{i1}(t)\\
d_{i2}(t) &= D_{i2} + \hat{d}_{i2}(t)\\
d_{i3}(t) &= D_{i3} + \hat{d}_{i3}(t)\\
d_{o1}(t) &= D_{o1} + \hat{d}_{o1}(t)\\
d_{o2}(t) &= D_{o2} + \hat{d}_{o2}(t)
\end{aligned}\right\} \quad (10)$$

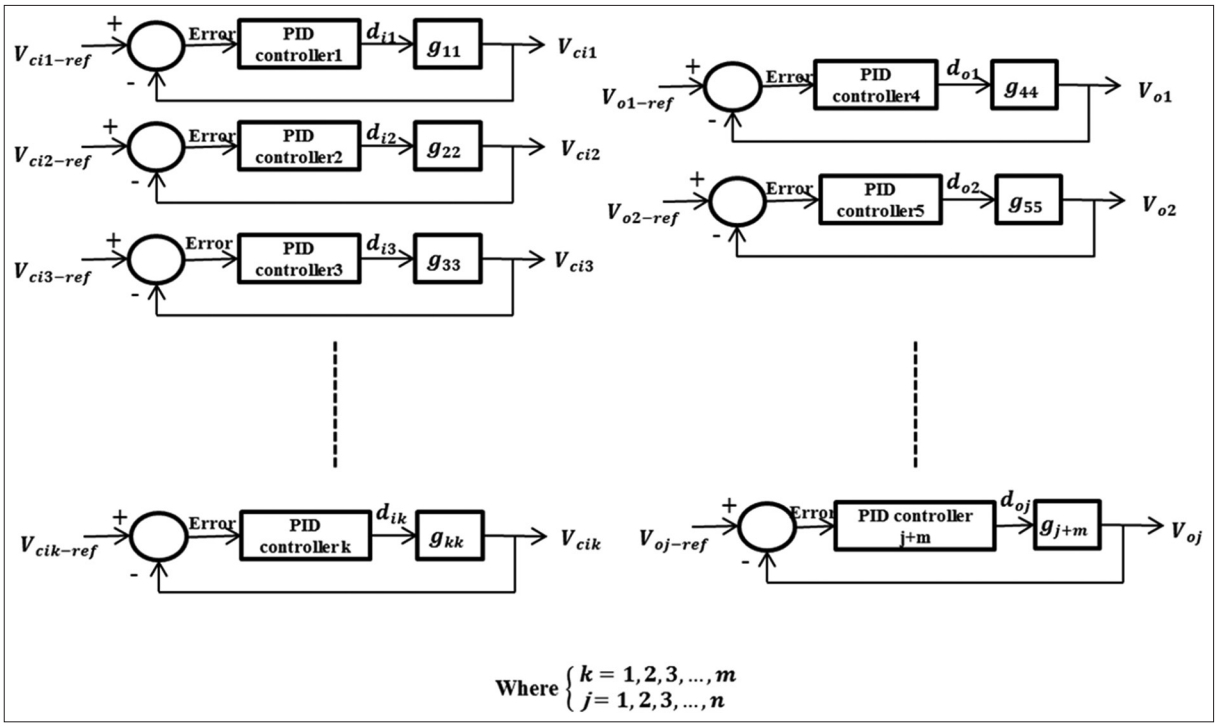

Figure 5. *The control block diagram of the proposed converter*

Where, iLi (t) and iLo (t) the input and output inductors' current and where the output capacitors' voltage v_{o1} (t) and v_{o2} (t) are state variables. Substitutes (10) into (6-9), then the averaging model is applied and multiplied by its corresponding duty cycle value. Hence, the system can be represented in a matrix form using a state-space averaging model. The state-space model takes the following form:

$$\left.\begin{aligned} \frac{dX}{dt} &= AX+BU \\ Y &= CX+DU \end{aligned}\right\} \tag{11}$$

Where, X is a matrix containing the state variables, U is a matrix containing the control inputs $\hat{d}_{i1}(t), \hat{d}_{i2}(t), \hat{d}_{i3}(t), \hat{d}_{o1}(t), \hat{d}_{o2}(t)$, and Y is a matrix containing the system outputs $\hat{v}_o(t), \hat{v}_{o1}(t), \hat{v}_{o2}(t)$.

Matrixes X, Y, and U take following form:

$$X = \begin{bmatrix} \hat{i}_{Li1}(t) \\ \hat{v}_{ci1}(t) \\ \hat{i}_{Li2}(t) \\ \hat{v}_{ci2}(t) \\ \hat{i}_{Li3}(t) \\ \hat{v}_{ci3}(t) \\ \hat{i}_{Lo1}(t) \\ \hat{v}_{co1}(t) \\ \hat{i}_{Lo2}(t) \\ \hat{v}_{co2}(t) \end{bmatrix}, Y = \begin{bmatrix} \hat{v}_{ci1}(t) \\ \hat{v}_{ci2}(t) \\ \hat{v}_{ci3}(t) \\ \hat{v}_{o1}(t) \\ \hat{v}_{o2}(t) \end{bmatrix}, U = \begin{bmatrix} \hat{d}_{i1}(t) \\ \hat{d}_{i2}(t) \\ \hat{d}_{i3}(t) \\ \hat{d}_{o1}(t) \\ \hat{d}_{o2}(t) \end{bmatrix}$$

The transfer function matrix of the converter is obtained from the small-signal model from matrices A, B, C, and D as follows:

$$G = C(SI-A)^{-1}B+D \tag{12}$$

The rank of transfer function matrix depends on the control variables; so according to the number of control variables, the rank of transfer function matrix G is 5×5

Where,

$$y = Gu \tag{13}$$

$$\begin{bmatrix} y_1 \\ y_2 \\ y_3 \\ y_4 \\ y_5 \end{bmatrix} = \begin{bmatrix} g_{11} & g_{12} & g_{13} & g_{14} & g_{15} \\ g_{21} & g_{22} & g_{23} & g_{24} & g_{25} \\ g_{31} & g_{32} & g_{33} & g_{34} & g_{35} \\ g_{41} & g_{42} & g_{43} & g_{44} & g_{45} \\ g_{51} & g_{52} & g_{53} & g_{54} & g_{55} \end{bmatrix} \begin{bmatrix} u_1 \\ u_2 \\ u_3 \\ u_4 \\ u_5 \end{bmatrix}$$

Where, y and u are the system output and input vectors, respectively, and component g_{ij} represents the transfer function between y_i and u_j. Hence, there are five transfer functions as follows:

$$g_{11} = \frac{\hat{v}_{ci1}}{\hat{d}_{i1}} = \frac{v_{i1}}{\left((1-D_{i1})(1+\frac{L_{i1}C_{i1}}{(1-D_{i1})^2})S^2\right)} \tag{14}$$

$$g_{22} = \frac{\hat{v}_{ci2}}{\hat{d}_{i2}} = \frac{v_{i2}}{\left((1-D_{i2})(1+\frac{L_{i2}C_{i2}}{(1-D_{i2})^2})S^2\right)} \tag{15}$$

$$g_{33} = \frac{\hat{v}_{ci3}}{\hat{d}_{i3}} = \frac{v_{i3}}{\left((1-D_{i3})(1+\frac{L_{i3}C_{i3}}{(1-D_{i3})^2})S^2\right)} \tag{16}$$

$$g_{44} = \frac{\hat{v}_{o1}}{\hat{d}_{o1}} = \frac{V_o(1-\frac{L_{o1}}{(1-D_{o1})^2 R_{L1}}S)}{\left((1-D_{o1})(1+\frac{(1-D_{o1})^2 R_{L1}\sqrt{\frac{C_{o1}}{L_{o1}}}}{\sqrt{L_{o1}C_{o1}}})S+\frac{L_{o1}C_{o1}}{(1-D_{o1})^2}S^2\right)} \tag{17}$$

$$g_{55} = \frac{\hat{v}_{o2}}{\hat{d}_{o2}} = \frac{V_o(1-\frac{L_{o2}}{(1-D_{o2})^2 R_{L2}}S)}{\left((1-D_{o2})(1+\frac{(1-D_{o2})^2 R_{L2}\sqrt{\frac{C_{o2}}{L_{o2}}}}{\sqrt{L_{o2}C_{o2}}})S+\frac{L_{o2}C_{o2}}{(1-D_{o2})^2}S^2\right)} \tag{18}$$

In this paper, the simulation results for three different input DC sources chosen within these ranges (V_{i1} = (200-500)V, V_{i2} = (350-875) V, and V_{i3} = (250-625) V) as an example of a different wind turbines DC voltage levels. Two output DC voltages are obtained using the integration of PID controllers. The values of the converter parameters the inductors L and the capacitors C have been obtained as discussed in our previous paper [8]. The controller has been designed in such a way to provide the following requirements, for the DC bus voltage, e.g. V_o = 4 kV,V_{o1}=8 kV and V_{o2}=11 kV. Hence, by controlling the bus DC voltage V_o through the PID controllers on the first stage of the designed converter to adapt itself as these inputs changes, thus the next stage will provide controlling the output DC voltages as the load changes. Figure 6 depicts the simulation results using MATLAB software of three-input and two-output DC-DC boost converter including the load and input sources variations to test the performance of the closed-loop control.

According to the results obtained from the simulation of a three-input and two-output DC-DC converter model associated with PID controllers, these results demonstrate the flexibility and robustness of the designed controller. The DC voltage Vo remains fixed as the input sources reduced by 20% and when the load changes by 50% with no

overshoot and with small peak to peak ripple voltage $V_{o_{(ripple)(p-p)}} = 20$ volts.

Similarly, the performance of the designed controller with the output voltages V_{o1} and V_{o2} has been tested as shown in Figure 6b and the controller demonstrates its flexibility and robustness in terms of the ability of the controller to keep the output voltages V_{o1} and V_{o2} fixed when the loads or the inputs changes with a good performance, i.e., 9.3% overshoot peak for V_{o1} and 7.2% for the second output V_{o2}, as well as small peak current and voltage ripple where

$$V_{o1_{(ripple)(p-p)}} = V_{o2_{(ripple)(p-p)}} = 40\,V$$

and

$$I_{o1_{(ripple)(p-p)}} = I_{o2_{(ripple)(p-p)}} = 200\,mA$$

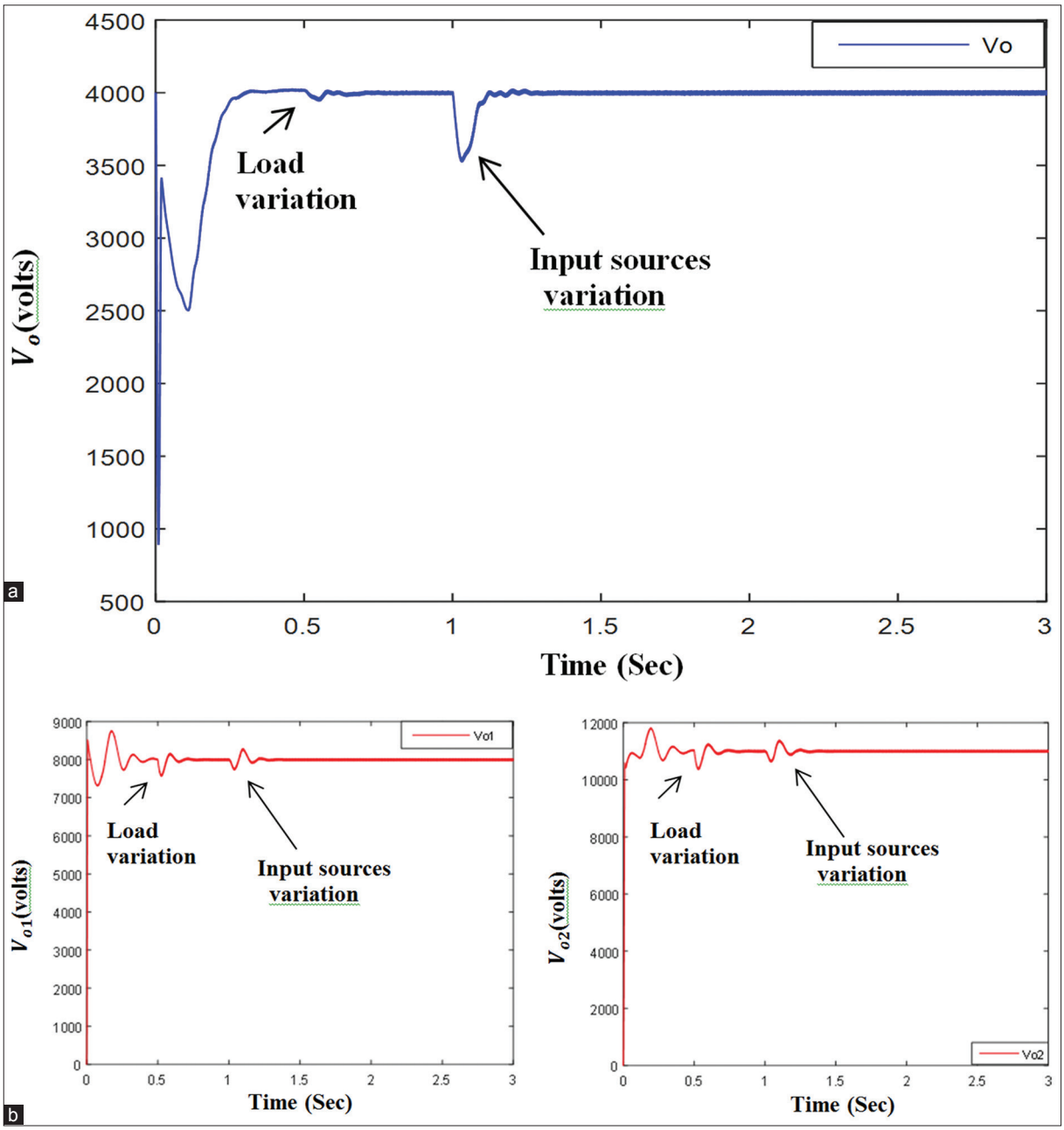

Figure 6. *Depicts the proposed converter output DC voltage results V_o = 4kV, V_{o1} = 8kV, V_{o2} = 11kV. (a) The bus DC voltage Vo with load variation at t=0.5 s and with input sources variation at t=1 s, (b) the output DC voltage V_{o1} and V_{o2} with load variation at t=0.5 s and with input sources variation at t=1 s*

Table 1. *Effects of the PID controller action on the time response curve specifications*

The time response curve specifications	Without the PID controller action	With the PID controller action
P.O	$P.O_{vo1} = 83.9\%$ overshooting $P.O_{vo2} = 154.7\%$ overshooting	$P.O_{vo1} = 9.3\%$ overshooting $P.O_{vo2} = 7.2\%$ overshooting
Rise time (s)	$t_{r\text{-}vo1} = 0.007$ $t_{r\text{-}vo2} = 0.013$	$t_{r\text{-}vo1} = 0.004$ $t_{r\text{-}vo2} = 0.007$
Settling time (s)	$t_{s\text{-}vo1} = 0.43$ $t_{s\text{-}vo2} = 0.5$	$t_{s\text{-}vo1} = 0.43$ $t_{s\text{-}vo2} = 0.46$
Steady-state error (%)	$S.S.e_{vo1} = 3.75$ $S.S.e_{vo2} = 6.36$	$S.S.e_{vo1} = 0$ $S.S.e_{vo2} = 0$
Peak-to-peak ripple voltage (volts)	$V_{o1(ripple)(p\text{-}p)} = 100$ $V_{o2(ripple)(p\text{-}p)} = 160$	$V_{o1(ripple)(p\text{-}p)} = 40$ $V_{o2(ripple)(p\text{-}p)} = 40$

P.O.: Percentage overshoot

The PID controller action has improved the output curve response as the percentage overshoot for each output has been reduced; also, the rise time has been decreased by almost 50% of its original value without using PID controller. The steady-state error has been eliminated due to the integration component of the PID controller.

Table 1 summarizes the effects of the PID controller action on the response curve. A comparison has been made between the time response specification curve with and without the PID controller action.

Hence, the designed controller has demonstrated that it has a good performance under input and load variations, as well as being adaptable.

4. CONCLUSION

In this study, a new MIMO DC-DC boost converter with the advantages of simple configuration, fewer components, and high conversion ratio for medium to high voltage applications is proposed. The mathematical representations of the proposed MIMO converter for ideal and non-ideal converter have been presented. The operation principles and the switching states with the dynamic modeling of the proposed converter have been provided. To verify the performance of the designed converter, MATLAB/SIMULINK simulations have been performed.

The results have proven the effectiveness of multi input sources integration; in terms of flexibility and reliability. Also demonstrated in the robustness of the designed controller through the simulation; where the controller automatically adapts the duty ratios of the power switches to achieve the predefined output voltages as the demand or the supply changes.The performance of designed controller provides fixed output voltages with ripple factor in order of 0.2% and with 100 mA peak ripple output currents. In addition, no overshoot in DC bus voltage response curve has been obtained also 9.3% and 7.2% overshoot peak for V_{o1} and V_{o2}, respectively.

To conclude, the controlled converter achieves a constant 8 kV, 11 kV for the two outputs from three DC input sources at an operating frequency of 1 kHz. The results prove the flexibility and reliability of the proposed converter and the simplicity of designing robust PID controllers to achieve a constant DC output voltage in different scenarios under inputs and load variations.

5. REFERENCES

[1] M.Biswal (2011), 'Control techniques for DC-DC buck converter with improved performance' National Institute of technology Rourkela, India.

[2] N. Mohan, T. M. Undeland and W. P. Robbins (1995), *Power Electronics Converters, Applications and Design,* Wiley, New York.

[3] M. K. Kazimierczuk (1988), Design-oriented analysis of boost zero-voltage- switching resonant DC/DC converter, *IEEE Trans. Power Electron*., **3**(2), 126-136.

[4] C. Buccella, C. Cecati and H. Latafat (2012), Digital control of power converters—A survey, *IEEE Trans. Industr. Inform.*, **8**(3), 437-447.

[5] J.Li (2009), 'Current-mode control: modelling and its digital application', Virginia polytechnic Institute and state university, Virginia, USA.

[6] L. Guo, J. Y. Hung, S. Member and R. M. Nelms (2009), Evaluation of DSP-based PID and fuzzy controllers for DC–DC converters, *IEEE Trans. Industr. Electron.*, **56**(6), 2237-2248.

[7] J. L. Calvo-Rolle and E. Corchado (2014), A bioinspired knowledge system for improving combined cycle plant control tuning, *Neurocomputing*, **126**, 95-105.

[8] M. Alzgool, G. Alzghoul, H. Nouri and C. Toomer (2016), A Novel Multi-Inputs-Single-Output DC Transformer Topology. *51st International Power Engineering Conference, ISEC Coimbra Portugal.*